DOI https: //doi. org/10.1007/s11595-020-2352-z

Microstructure, Mechanical, and Thermal Properties of B_4C-TiB_2-SiC Composites Prepared by Reactive Hot-pressing

CAO Yaoqin[1], HE Qianglong[2*], WANG Weimin[2*]

(1.China Helicopter Research and Development Institute, Tianjin 300450, China; 2.The State Key Laboratory of Advanced Technology for Materials Synthesis and Processing, Wuhan University of Technology, Wuhan 430070, China)

Abstract: B_4C-TiB_2-SiC composites with excellent properties were prepared by reactive hot-pressing using B_4C, TiC, and Si powders as the raw materials. The phase transition process was investigated by heating the powder mixture to different temperatures and combined with XRD tests. TiB_2 and SiC phases were synthesized through an *in situ* reaction, and the mechanical and thermal properties were improved simultaneously. Microstructure and mechanical properties were also studied, and the 60wt% B_4C-21.6wt% TiB_2-18.4wt% SiC composite showed a relative density of 99.1%, Vickers hardness of 34.6 GPa, flexural strength of 582 MPa, and fracture toughness of 5.08 MPa·$m^{1/2}$. In addition, the values of thermal conductivity and thermal expansion coefficient were investigated, respectively.

Key words: B_4C-TiB_2-SiC; reactive hot pressing; microstructures; mechanical properties; thermal properties

1 Introduction

Boron carbide (B_4C) has many excellent properties, such as high hardness (37.7 GPa), low density (2.52 g/cm^3), high melting point (2447 ℃), high elastic modulus (450 GPa), high fever electromotive force, good chemical stability, high neutron absorption cross section, good shock resistance and excellent wear resistance. It can have all the above excellent properties at the same time, which is not possessed by any other ceramic material. Therefore, boron carbide ceramics are considered a strategic material and are widely used in light armor, grinding and cutting tools, ceramic bearings, injector nozzles, nuclear industry and high temperature thermocouples[1-3].

Although boron carbide ceramics have these excellent properties, due to the close proximity of boron (B) and carbon (C) atoms, the different in electronegativity between them is very small, and a strong covalent bond is formed with a high proportion of covalent bonds. In addition, boron carbide has a high melting point and a low self-diffusion coefficient, and there is usually a thin surface oxide layer (B_2O_3) on the surface of boron carbide powder particles. All these factors will hinder the densification process of boron carbide, making the sintering of boron carbide extremely difficult, and also making the fracture toughness of boron carbide as low as 2.2 MPa·$m^{1/2}$[4-7]. Therefore, the application of boron carbide ceramics is greatly limited.

B_4C ceramics are usually toughened by adding additives. The main methods are phase transition toughening, fiber toughening and second phase particle toughening[8-10]. The second phase particle toughening method has the characteristics of simple process and good effect, so it has attracted extensive attention. Among the second phase particles, the most ideal choice is TiB_2 and SiC, which can effectively improve the sintering and mechanical properties of the materials while maintaining the high hardness and low density of the B_4C matrix[11-16]. Moreover, TiB_2 particles can greatly improve the electrical conductivity of the materials, making it possible to use electrical discharge machining (EDM) to process the materials. In addition, SiC can effectively improve the oxidation resistance of the material, due to the oxidation product SiO_2 of SiC at high temperature can effectively repair the cracks and

(Received: June 16, 2020; Accepted: Oct. 9, 2020)

CAO Yaoqin(曹瑶琴): Researcher; E-mail: caoyq001@avic.com

*Corresponding authors: HE Qianglong(何强龙): E-mail: shsqlhe@whut.edu.cn; WANG Weimin(王为民): Prof.;E-mail: shswmwang@whut.edu.cn

Funded by the National Key Research and Development Plan of China (2017YFB0310400), and the National Natural Science Foundation of China (5167020705)

holes formed by oxidation damage of the material[17-19]. Therefore, B_4C-TiB_2-SiC composites are expected to become multifunctional ceramic materials with excellent comprehensive performance.

The particle size of the additive powders has an important influence on the sintering performance and mechanical properties of the composite ceramics, fine particle additives are beneficial to sintering and mechanical properties of the composite ceramics. However, commercial TiB_2 powders generally have particle sizes close to 10 μm. Reactive sintering provides a way to obtain powders with fine particle sizes even from coarse precursors[20]. Recently, fine TiB_2 particles were introduced into the B_4C matrix by reaction (1)[21,22], and B_4C-SiC composite ceramics were prepared by B_4C-SiO_2-C or B_4C-polycarbosilane starting powders[23-25].

$$B_4C + 2TiO_2 + 3C \rightarrow 2TiB_2 + 4CO\ (g) \qquad (1)$$

All the above preparation methods would generate gas during the sintering process, which is adverse to the densification process of the composite ceramics. In this study, both TiB_2 and SiC particles were introduced into the B_4C matrix by a solid reaction (2) without gas formation. And the reaction process, microstructures, mechanical and thermal properties of the B_4C-TiB_2-SiC composite ceramics fabricated by reactive hot presssing was investigated.

$$B_4C + 2TiC + 3Si \rightarrow 2TiB_2 + 3SiC \qquad (2)$$

2 Experimental

The starting materials used in this study were commercial B_4C powders (Mudanjiang Jinggangzuan Boron Carbide Co. Ltd., China) with a purity of 97% and a mean particle size of 2.5 μm, TiC powders (Aladdin Co. Ltd., China) with a purity of 99% and a mean particle size of 3 μm, Si powders (Aladdin Co. Ltd., China) with a purity of 99.9 % and a mean particle size of 1 μm. The starting powder mixtures of 84.3wt% B_4C-9.2wt% TiC-6.5wt% Si and 68.5wt% B_4C-18.5wt% TiC-13.0wt% Si were mixed in a polythylene bottle with ethanol and agate balls for 24 h by a roller mill (GMJ/B, Xianyang Jinhong General Machinery Co. Ltd., China). The slurry obtained after mixing was separated from the agate ball by funnel and transferred into the eggplant bottle. After that, the slurry was treated with solid-liquid separation by a rotating evaporator (R, Shanghai SENCO Technology Co. Ltd., China), the water bath temperature of the rotary evaporator is 60 ℃ and the rotation speed is 50 rpm. Next the powder mixture was placed in a vacuum drying chamber (DZF-6050, Shanghai Jinghong Laboratory Equipment Co. Ltd., China) at 60 ℃ for 24 h. Then the as-received powder mixtures were sieved through a 200-mesh sieve to minimize the powder agglomeration.

Weigh the powder mixture of 18 g and pour it into a graphite mold with an inner diameter of 48 mm, in order to avoid direct contact between the powder and the graphite die, the powder and the die were separated by 0.2 mm graphite paper. Then the samples were sintered at a temperature of 1950 ℃ under a uniaxial pressure of 30 MPa by a vacuum hot-pressing furnance (916G, Thermal Technology Inc, USA). The heating rate during the low temperature stage before 1 400 ℃ in vacuum was 20 ℃/min, and then 10 ℃/min to 1950 ℃ in an argon atmosphere with a dwelling time of 1 h. Afterwards, removed the applied machanical pressure and stopped heating to allow the sample to cool to room temperature by the cooling water. The sample of 80wt%B_4C-10.8wt%TiB_2-9.2wt%SiC reacted from 84.3wt%B_4C-9.2wt%TiC-6.5wt% Si was marked as BTS20 and the sample of 60wt%B_4C-21.6wt%TiB_2-18.4wt%SiC reacted from 68.5wt%B_4C-18.5wt%TiC-13.0wt%Si was marked as BTS40. In addition, the powder mixtures were heated to 1 000, 1 100, 1 200, 1 300, and 1 400 ℃ respectively without any dwelling time in order to study the reaction process.

The bulk density of the sintered sample was measured by the Archimedes method with distilled water as the immersing medium. The theoretical density was measured via the rule of mixtures based on the densities of 2.52 g/cm^3 for B_4C, 4.52 g/cm^3 for TiB_2, and 3.21 g/cm^3 for SiC. And the relative density was calculated by the bulk density and the theoretical density. The flexual strength was measured through three-point-bending test on specimens (3 mm × 4 mm × 36 mm) with a span of 30 mm and a loading rate of 0.5 mm/min and the fracture toughness was measured via single-edge notched beam test using samples of size 2.5 mm× 5 mm × 25 mm (notch depth = 2.5 mm) with a span of 20 mm and a loading rate of 0.05 mm/min. The test of bending strength and fracture toughness was completed by the ceramic test system (MTS810, MTS, USA) and the values were determined based on the measurements of five bars. The hardness was measured by a Vickers hardness tester (430SVD, Wolpert, USA) with an applied load of 9.8 N for a dwelling time of 15 s on a polished surface.

The phase composition was characterized by X-ray diffraction (XRD, Rigaku Ultima III, Japan) with

Cu-Kα radiation. The polished, etched and fractured surfaces of B_4C-TiB_2-SiC composites were investigated by scanning electron microscope (SEM, Hitachi 3400, Japan). The polished surfaces were electrochemically etched in 1% KOH solution with a current density of 0.1 A/cm^2 for 20 s. Image analysis software of ImageJ was used to estimate the average grain sizes that were obtained by measuring more than 50 randomly selected grains from etched surface SEM images. The elemental analysis of the composites was investigated by electron probe micro-analyzer (EPMA, JXA-8230, Japan) equipped with wavelength dispersive spectroscopy (WDS) and energy dispersive spectroscopy (EDS). The thermal diffusivity (k) of the B_4C-TiB_2-SiC composite was tested by the laser flash method using a laser thermal conductivity testing instrument (LFA457, Netzsch, Germany) for square specimens (10 mm × 10 mm × 2.5 mm). The specific heat (c) of each phase (B_4C, TiB_2, and SiC) was evaluated from the chemical thermodynamics simulation software of HSC Chemistry 6, and the specific heat (c) of the composite was calculated using the rule of mixtures by considering the weight fraction. Then, the thermal conductivity (λ) could be calculated by Eq. (1):

$$\lambda = kcd \tag{1}$$

where, d is the density of the composite. The coefficient of thermal expansion (CTE) was measured by an autometic thermal mechanical analyzer (DIL402C, Netzsch, Germany) from 20 ℃ to 1 000 ℃ using rectangular samples (3.5 mm × 3.5 mm × 14 mm). The changes in length (ΔL) with increasing temperature were recorded in succession and the value of CTE (α) was calculated by Eq.(2):

$$\alpha = \Delta L / (L_0 \cdot \Delta L) \tag{2}$$

where, L_0 is the length of the sample at the initial temperature, and ΔL is the change in the length when the temperature varied ΔT.

3 Results and discussion

3.1 Reaction process

The effect of temperature on the phase composition of the powder mixtures during the heating process is shown in Fig.1.

The XRD patterns of the original mixtures was almost the same with that heated to 1 000 ℃, there had no obvious change on the XRD intensity of each phase, indicating that no reaction happened before 1 000 ℃. When the temperature increased to 1 100 ℃, it could be observed clearly that the XRD intensity of TiC phase had a certain diminishing, and a deformation of the B_4C peak occurred near 35°. It can be speculated that TiB_2 phase had already been produced, but the peak of TiB_2 could not be detacted visibly by XRD due to the content of the produced TiB_2 was very few or the crystallization was quite poor caused by its tiny particle size. Peaks of TiB_2 phase could be observed as the temperature reached 1 200 ℃. When the temperature come to 1 300 ℃, the intensity of the TiB_2 phase enhanced mildly and the Si phase weakened moderately, at the same time, the peak of SiC phase was detected. When the temperature ascent to 1 400 ℃, the XRD intensity of the TiB_2 phase increased significantly, the TiC and Si phases were completely reacted and their XRD peaks disappeared, in the meantime sharp peaks of the SiC phase were observed. The phase composition of the powder mixtures reacted at 1 400 ℃ was almost the same as the final product that sintered at 1 950 ℃ for 1h. Indicating that the B_4C-TiC-Si system reacted completely at 1 400 ℃, all of the TiC, Si conversed into TiB_2, SiC and no other product was found.

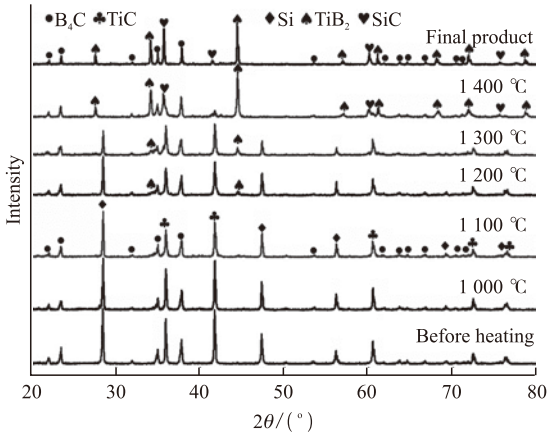

Fig.1 XRD patterns of the powder mixtures heated to different temperatures

It could be seen from the XRD analysis above that the reaction process of the B_4C-TiC-Si system was completed step by step. TiB_2 phase and SiC phase generated slightly at 1 100 ℃ and 1 300 ℃, respectively. Then a great quantity of TiB_2 phase and SiC phase created until 1 400 ℃. The reasons for this phenomenon could be explained as follows: the substance transport rate of solid-state reaction is slow, what's more, the product layer of TiB_2 and C prevent B atoms diffusing into TiC to form more TiB_2. Vast TiB_2 and C produced until the Si melted between 1 300 ℃ to 1 400 ℃ that provided a new diffusion channel for B atoms, then sufficient C and Si created a large number of SiC, simi-

lar phenomena had been reported[26].

The overall reactive equations for the experiment is shown as reaction (2) and the reactions probablely occurred during the process are shown as reactions (3)-(6):

$$B_4C + 2TiC \rightarrow 2TiB_2 + 3C \quad (3)$$

$$Si + C \rightarrow SiC \quad (4)$$

$$B_4C + Si \rightarrow SiC + 4B \quad (5)$$

$$TiC + Si \rightarrow SiC + Ti \quad (6)$$

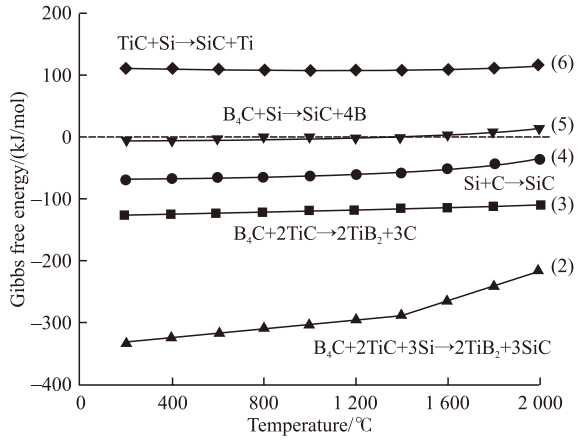

Fig.2 Gibbs free energy change of reactions (2)-(6)

The corresponding thermodynamics data of the reactive equations above are shown in Fig.2. The Gibbs free energy of the reaction that generated TiB_2 is much more negative than the reaction that created SiC, as a result, the temperature for the producing of TiB_2 (1 100 ℃) is lower than that of SiC (1 300 ℃). There are three potential reactions (4), (5), and (6) to creat SiC phase. Thermodynamic calculations suggest that only reactions (4) and (5) are thermodynamiclly favourable from 1 000 ℃ to 1 400 ℃, and the Gibbs free energy of reaction (4) is much more negative than reaction (5), showing that reaction (4) is more favourable than reaction (5). So the SiC phase is generated by the reaction of Si and C.

3.2 Microstructures

The elemental (Ti, Si, B, and C) distribution of the sample (BTS40) was analyzed via the EPMA equipped with WDS and EDS. The BSE image and the corresponding element mappings of this region are shown in Fig.3. Combined with the XRD results shown in Fig.1, we can conclude that the white areas where Ti and B concentrated on are TiB_2 phases, the grey areas where Si and C concentrated on are SiC phases and the dark areas where B and C concentrated on are B_4C phases. It can be judged from Fig.3 that TiB_2 and SiC phases are uniformly dispersed in the B_4C matrix.

Figs.4(a) and 4(c) show the polished surfaces of the BTS20 and BTS40 composites, respectively. The TiB_2 and SiC phases dispersed homogeneously in the B_4C matrix. A few black areas were formed from the particles being pulled out during the abrasion process and the subsequent incomplete polishing. The partial enlargements of Figs.4(a) and 4(c) are shown in Figs.4(b) and 4(d), indicating that the white and grey areas are not the grains growed up abnormally, but the aggregates composed of small grain size TiB_2 and SiC grains.

Fig.5 shows the etched microstructures of BTS20 and BTS40 composites. Some pores were formed by the chemical corroding of TiB_2 due to the weaker chemical stability and the higher conductivity of TiB_2. The grain sizes of B_4C grains were measured by Figs.4(a)-4(c) from 56 randomly selected grains that divided into four grous from small size to large size.

Fig.6 shows the grain sizes of B_4C grains of BTS20 and BTS40 composites, the mean sizes of B_4C grains in BTS20 and BTS40 are 3.72 μm and 3.38 μm, respectively. With the increasing of the TiB_2 and

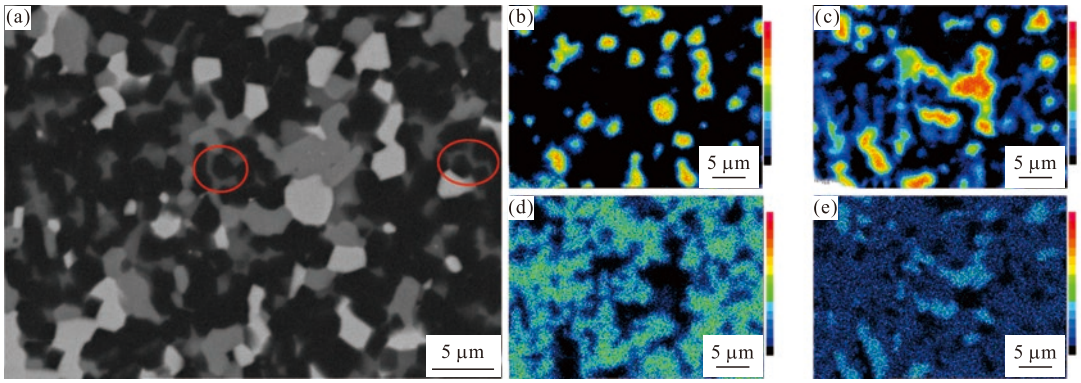

Fig.3 EPMA mapping images of the BTS40 composite: (a) Back scattering image; (b-e) The elemental distribution maps of Ti, Si, B, and C

SiC content, the grain size of B_4C became smaller due to the inhibiting effect of TiB_2 and SiC. TiB_2 grains mainly located at the junctions of the B_4C grains which can inhibit the growth of B_4C by the pinning effect. In addition, because of the C created by the reaction of B_4C and TiC distributed around the B_4C, forming the structure of the B_4C being half-surrounded by the SiC as shown in the red circle of Fig.3(a), so the growth of B_4C was further inhibited.

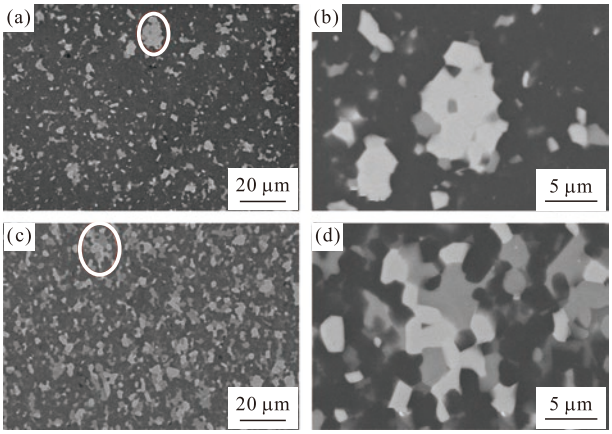

Fig.4 Polished surfaces and the partial enlarged BSE images of BTS20 (a, b) and BTS40 (c, d)

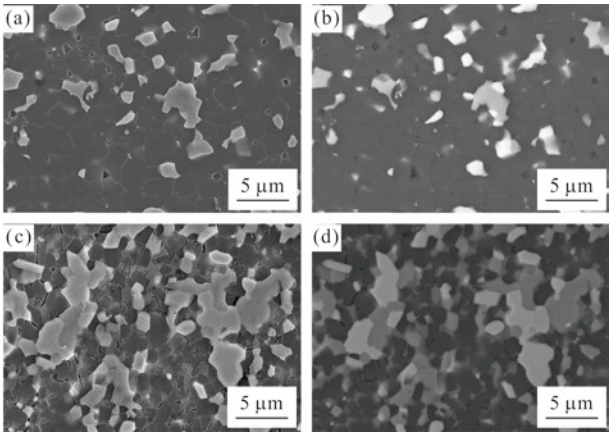

Fig.5 Etched surfaces and the BSE images of BTS20 (a, b) and BTS40 (c, d)

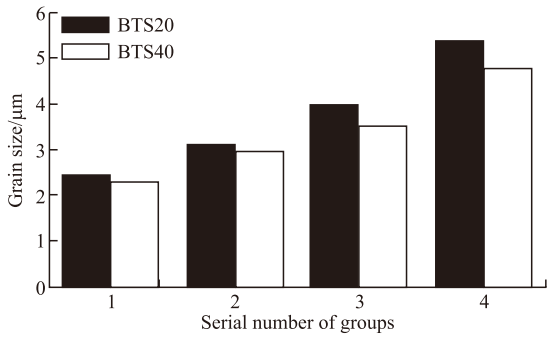

Fig.6 The grain sizes of B_4C grains of BTS20 and BTS40

The dence and rough fracture surface is shown in Fig.7(a), the phenomenon of grain pull-out and the mix mode of intergranular/transgranular fracture were observed which improved the fracture toughness. Fig.7(b) shows the crack propagation path, toughening mechanisms of crack deflection and crack bridging could be obsered. Crack deflection mainly occurred around TiB_2 phase result from the expansion coefficient mismatch between B_4C/ TiB_2 and SiC/ TiB_2.

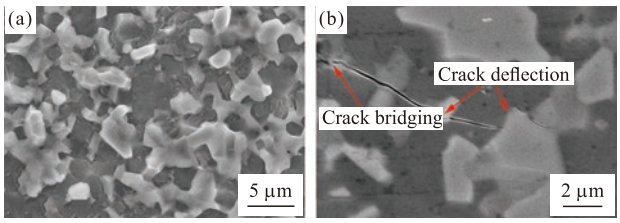

Fig.7 SEM images of BTS40 composite: (a) Fracture surface; (b) Polished surface with crack propagation

3.3 Mechanical and thermal properties

The mechanical properties of BTS20 and BTS40 are shown in Table 1. The BTS40 composite possessed the optimum properties with a relative density of 99.1%, hardness of 34.6 GPa, flexual strength of 582 MPa and fracture toughness of 5.08 MPa·$m^{1/2}$. The relative density, flexual strength and fracture toughness of the composite enhanced with the increasing of the generated TiB_2 and SiC, because of the fresh particles owned higher sintering activity and the smaller grain might improve both the flexual strength and fracture toughness. The hardness of BTS40 is lower than BTS20 due to the lower hardness of the TiB_2 and SiC phases than the B_4C matrix.

Table 1 Mechanical properties of the B_4C-TiB_2-SiC composite ceramics

Samples	Relative density/%	Hardness /GPa	Flexural strength /MPa	Fracture toughness /(MPa·$m^{1/2}$)
BTS20	98.5	35.8±0.5	517±27	4.59±0.45
BTS40	99.1	34.6±0.7	582±41	5.08±0.37

Fig.8(a) shows the specific heats (c) of B_4C, TiB_2, and SiC calculated by HSC Chemistry 6, and the specific heats of BTS20 and BTS40 were calculated based on the rule of mixture according to the weight fraction. Fig.8(b) shows the thermal diffusivity (k) of BTS20 and BTS40 tested by the laser flash method using Netzsch-457. The thermal conductivity had been calculated by Eq.(2): $\lambda=kcd$ and d was the density measured by Archimedes' principle at room temperature. Fig.8(c) shows the thermal conductivity of the BTS20, BTS40 composites and the reference values of B_4C[27], TiB_2[28] and SiC[29]. The thermal diffusivity of B_4C-TiB_2-SiC composite is determined by both electrons and phonons thermal transport mechanisms, thermal transport by

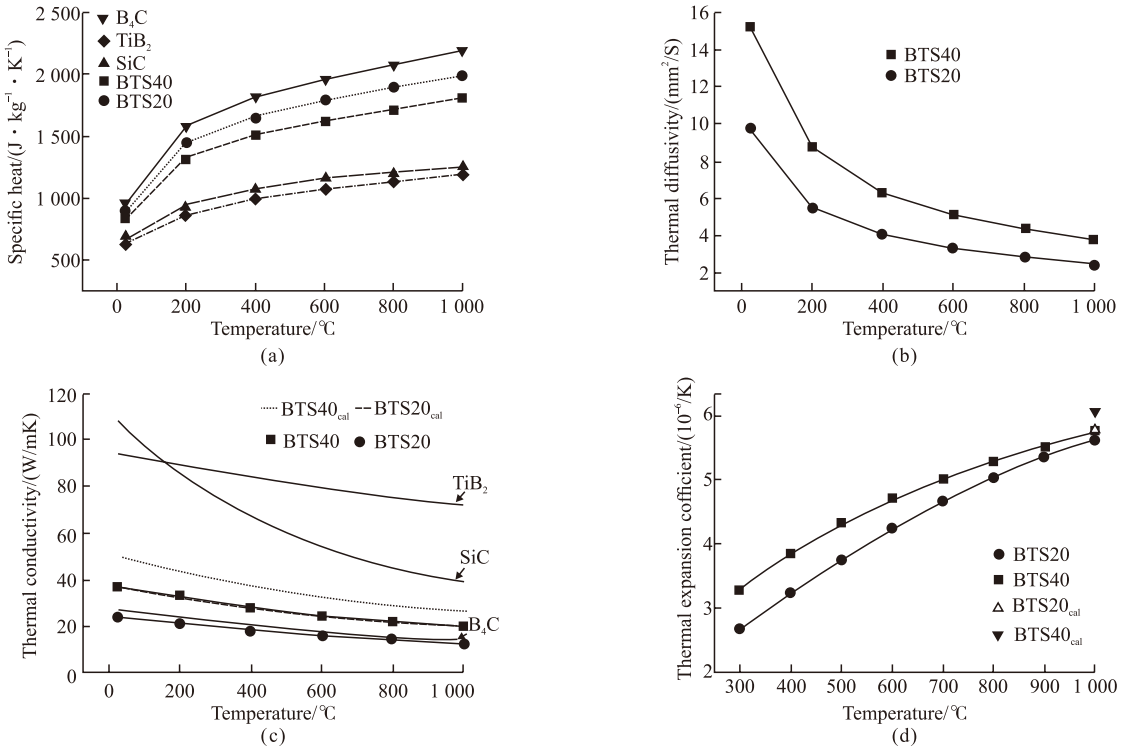

Fig.8 Thermal properties of BTS20 and BTS40 composites: (a) Specific heat; (b) Thermal diffusivity; (c) Thermal conductivity; (d) Thermal expansion coefficient

Table 2 Experimental (α) and theoretical (α_c) values of CTE (25 °C-1 000 °C, ×10^{-6} K) for BTS20 and BTS40

Sample	Experimental value/α	Theoretical value/α_c	α/α_c
BTS20	5.63	5.77	97.6%
BTS40	5.75	6.07	94.7%

electrons relying on the TiB_2 phase, thermal transport by phonons relying on the covalently bonded B_4C and SiC phases, and the thermal transporting by phonons has played the major role. It can be observed that the thermal conductivity decreased with the temperature increasing due to phonon-scattering. The measured values (λ) of the thermal conductivity are lower than the theoretical calculated values (λ_c) and the ratio λ/λ_c of BTS20 is lower than that of BTS40. The reasons may be: the content of TiB_2 and SiC in BTS20 is too little to form a continuous network structure, so the thermal transport is still mainly depend on the B_4C matrix; in addition, the relative density of BTS40 is higher than that of BTS20 which can also affect the result. Fig.8(d) shows the thermal expansion coefficients of the composites from 300 ℃ to 1 000 ℃ and the values calculated by the references at 1 000 ℃[30-32]. The results show that the CTE of the composites increased with the temperature rising. Further, the CTE value of BTS40 is higher than that of BTS20 due to the CTE of TiB_2 is much higher than B_4C and SiC.

Table 2 shows the measured values of CTE and the calculated values of CTE by volume fraction. The ratio α/α_c of BTS40 is lower than that of BTS20. The causes of this phenomenon may be that larger interfacial area lowered the CTE value of BTS40 resulted from the smaller matrix grain size of the composite; furthermore, higher content of TiB_2 leaded to more microcracks which could provided space for the expansion.

4 Conclusions

B_4C-TiB_2-SiC composites were *in situ* synthesized by hot pressing using B_4C, TiC, and Si as raw materials. Based on the XRD patterns and thermodynamic data, indicating that TiB_2 was synthesized by the reaction of B_4C and TiC; SiC was synthesized by the reaction of Si and C. The BTS40 composite showed the optimum mechanical and thermal properties: relative density of 99.1%, Vickers hardness of 34.6 GPa, flexural strength of 582 MPa and fracture toughness of 5.08 MPa·m$^{1/2}$; thermal conductivity of 36.91-19.94 W/mK from 25 ℃ to 1 000 ℃, thermal expansion coefficient of 5.81×10^{-6}/K(25 -1 000 ℃). The machanical and thermal properties of the composite increased with the content of TiB_2 and SiC increasing.

References

[1] Thévenot F. Boron Carbide-A Comprehensive Review[J]. *J. Eur. Ceram. Soc*., 1990, 6(4): 205-225

[2] Suri A, Subramanian C, Sonber J, *et al*. Synthesis and Consolidation of Boron Carbide: A Review[J]. *Int. Mater. Rev*., 2010, 55(1): 4-40

[3] Domnich V, Reynaud S, Haber RA, *et al.* Boron Carbide: Structure, Properties, and Stability under Stress[J]. *J. Am. Ceram. Soc*., 2011, 94(11): 3 605-3 628

[4] Zhang M, Yuan T, Li R, *et al.* Densification Mechanisms and Microstructural Evolution during Spark Plasma Sintering of Boron Carbide Powders[J]. *Ceram. Int*., 2018, 44(4): 3 571-3 579

[5] Lee H, Speyer RF. Pressureless Sintering of Boron Carbide[J]. *J. Am. Ceram. Soc.*, 2003, 86(9): 1 468-1 473

[6] Huang SG, Vanmeensel K, Malek OJA, *et al.* Microstructure and Mechanical Properties of Pulsed Electric Current Sintered B_4C-TiB_2 Composites[J]. *Mater. Sci. Eng. A*., 2011, 528(3): 1 302-1 309

[7] Xu CM, Cai YB, Flodström K, *et al.* Spark Plasma Sintering of B_4C Ceramics: The Effects of Milling Medium and TiB_2 Addition[J]. *Int. J. Refract. Met. Hard Mater*., 2012, 30(1): 139-144

[8] Lv M, Chen W, Liu C. Fabrication and Mechanical Properties of TiB_2/ZrO_2 Functionally Graded Ceramics[J]. *Int. J. Refract. Met. Hard Mater.*, 2014, 46: 1-5

[9] Zhang M, Zhang WK, Zhang YJ, *et al.* Fabrication, Microstructure and Mechanical Behavior of SiC_w-B_4C-Si Composite[J]. *Mater. Sci. Eng. A*., 2012, 552: 410-414

[10] Skorokhod V, Krstic VD. High Strength-High Toughness B_4C-TiB_2 Composites[J]. *J. Mater. Sci. Lett*., 2000, 19(3): 237-239

[11] He P, Dong S, Kan Y, *et al.* Microstructure and Mechanical Properties of B_4C-TiB_2 Composites Prepared by Reaction Hot Pressing using Ti_3SiC_2 as Additive[J]. *Ceram. Int.*, 2016, 42(1): 650-656

[12] Yamada S, Hirao K, Yamauchi Y, *et al.* High Strength B_4C-TiB_2 Composites Fabricated by Reaction Hot-Pressing[J]. *J. Eur. Ceram. Soc*., 2003, 23(7): 1 123-1 130

[13] He QL, Wang AY, Liu C, *et al.* Microstructures and Mechanical Properties of B_4C-TiB_2-SiC Composites Fabricated by Ball Milling and Hot Pressing[J]. *J. Eur. Ceram. Soc*., 2018, 38(7): 2 832-2 840

[14] Moshtaghioun BM, Ortiz AL, García DG, *et al*. Toughening of Super-Hard Ultra-Fine Grained B_4C Densified by Spark-Plasma Sintering via SiC Addition[J]. *J. Eur. Ceram. Soc*., 2013, 33(8): 1 395-1 401

[15] Moradkhani A, Baharvandi H. Mechanical Properties and Fracture Behavior of B_4C-Nano/Micro SiC Composites Produced by Pressureless Sintering[J]. *Int. J.Refract. Met. Hard Mater*., 2018, 70: 107-115

[16] He QL, Xie JJ, Wang AY, *et al.* Effects of Boron Carbide on The Microstructures and Mechanical Properties of Reactive Hot-Pressed B_xC-TiB_2-SiC Composites[J]. *Ceram. Int.*, 2019, 45(16): 19 650-19 657

[17] Tomlinson WJ, Jupe KN. Strength and Microstructure of Electro Discharge-Machined Titanium Diboride[J]. *J. Mater. Sci. Lett*., 1993, 12(6): 366-378

[18] Li WJ, Tu R, Goto T. Preparation of TiB_2-SiC Eutectic Composite by An Arc-Melted Method and Its Characterization[J]. *Mater. Trans*., 2005, 46(11): 2504-2508

[19] Tu R, Hirayama H, Goto T. Preparation of ZrB_2-SiC Composites by Arc Melting and Their Properties[J]. *J. Ceram. Soc. Jpn.*, 2008, 116(1351): 431-435

[20] Zou J, Liu J, Zhao J, *et al*. A Top-Down Approach to Density ZrB_2-SiC-BN Composites with Deeper Homogeneity and Improved Reliability[J]. *Chem. Eng. J*., 2014, 249: 93-101

[21] Yue X, Zhao S, Lu P, *et al.* Synthesis and Properties of Hot Pressed B_4C-TiB_2 Ceramic Composite[J]. *Mater. Sci. Eng. A*., 2010, 527 (27-28): 7 215-7 219

[22] Huang S, Vanmeensel K, Biest OV, *et al.* In Situ Synthesis and Densification of Submicrometer-Grained B_4C-TiB_2 Composites by Pulsed Electric Current Sintering[J]. *J. Eur. Ceram. Soc*., 2011, 31(4): 637-644

[23] Sahin FC, Apak B, Akin I, *et al.* Spark Plasma Sintering of B_4C-SiC Composites[J]. *Solid. State. Sci*., 2012, 14(11-12): 1 660-1 663

[24] Du XW, Zhang ZX, Wang WM, *et al.* Microstructure and Properties of B_4C-SiC Composites Prepared by Polycarbosilane-Coating/B_4C Powder Route[J]. *J. Eur. Ceram. Soc*., 2014, 34(5): 1 123-1 129

[25] Zhou Y, Ni D, Kan Y, *et al.* Microstructure and Mechanical Properties of Reaction Bonded B_4C-SiC Composites: The Effect of Polycarbosilane Addition[J]. *Ceram. Int.*, 2017, 43(8): 5 887-5 895

[26] Zhang Z, Xu C, Du X, *et al*. Synthesis Mechanism and Mechanical Properties of TiB_2-SiC Composites Fabricated with The B_4C-TiC-Si System by Reactive Hot Pressing[J]. *J. Alloy. Compd*., 2015, 619: 26-30

[27] Xie Z. *Structure Ceramics*[M]. Beijing: Tsinghua University Press, 2011: 486-496

[28] Königshofer R, Fürnsinn S, Steinkellner P, *et al*. Solid-State Properties of Hot-Pressed TiB_2 Ceramics[J]. *Int. J. Refract. Met. Hard Mater.*, 2005, 23(4-6): 350-357

[29] Sigl LS. Thermal Conductivity of Liquid Phase Sintered Silicon Carbide[J]. *J. Eur. Ceram. Soc*., 2003, 23(7): 1 115-1 122

[30] Zou J, Zhang G, Kan Y. Pressureless Densification and Mechanical Properties of Hafnium Diboride Doped with B_4C: From Solid State Sintering to Liquid Phase Sintering[J]. *J. Eur. Ceram. Soc*., 2010, 30(12): 2 699-2 705

[31] Skaar EC, Croft WJ. Thermal Expansion of TiB_2[J]. *J. Am. Ceram. Soc*., 1973, 56(1): 45

[32] Munro RG. Material Properties of A Sintered Alpha-SiC[J]. *J. Phy. Chem. Ref. Data.*, 1997, 26(5): 1 195-1 203